2017 IEEE International Conference on Robotics and Automation (ICRA)
Singapore, May 29 - June 3, 2017

# High-rate controlled turning with a pair of miniature legged robots*

TaeWon Seo, *Member, IEEE,* Carlos S. Casarez, Ronald S. Fearing

***Abstract*—Legged robots can explore unstructured environments more effectively than wheeled robots, but high turning rate tracking is still a challenging problem, particularly on varying surfaces. Previous steering methods with small robots have shown high turn rates, but usually only on a limited set of surfaces. This paper proposes a new method for steering a miniaturized legged robot by cooperation between two robots connected by a compliant joint, creating a 73 gram, 12 legged robot. Detailed design issues and an empirical verification are presented for several cooperation strategies, including changing velocities of the 4 sets of leg triples. The robots use their combined traction forces to turn at better than 50 degrees/sec at 1 m/sec on various surfaces. Closed-loop steering using a differential drive strategy is implemented on the connected robots to track a "figure 8" trajectory on a tile surface.**

## I. Introduction

Light-weight legged millirobots have been developed for search and rescue missions in hazardous and unstructured environments [1]. The robots have functional advantages of high speed [2], robustness to external impact [3], and the ability to overcome obstacles [4]. The robots can also be made cheaply and quickly with little resources, and researchers are trying to use groups of disposable robots to complete a single mission [5, 6]. Due to their agility in unstructured environments, these robots have higher potential to complete search and rescue missions than wheeled or tracked robots, which were not successful in similar missions related to the Fukushima nuclear accident [7].

Many different legged millirobots have been suggested by researchers and manufactured by Smart Composite Manufacturing (SCM) [8]. The SCM process combines one compliant polymer sheet between two hard sheets such as cardboard or carbon fiber sheets. After the process, the robot can be assembled by folding the sheet manually or automatically [9]. Important examples of such robots are DASH [3], VelociRoACH [2], Myriapod [10], and HAMR [9]. Recently, the possibility of mass producing robust miniaturized legged robots has been increased by developments in design processes [1], automatic pop-up assembly [9], and materials [2].

Turning is one critical issue for using legged millirobots in search and rescue missions. One method for turning nonholonomic wheeled or legged robots is skid steering, which involves different speeds of the left and right wheels or legs [11]. This method is very simple and intuitive, but it does not capture the effects of intermittent/slipping leg contact. Recently, Haldane and Fearing [12] suggested a turning method that changes the phase of the left and right legs at the same frequency. This method allows the robot to steer by rolling oscillation of the body but shows good performance on only smooth surfaces. Lee and Fearing [13] proposed a turning method using anisotropic spines on feet, but the method cannot control the turning direction without swapping claws and is only effective on rough surfaces.

Tails have received extensive interest from researchers in biology and robotics. Tails help living creatures to control their posture [14, 15] and increase stability [16, 17]. Bio-inspired turning methods have been suggested recently using different types of a tails. A tail with inertia was used to steer a legged millirobot on a smooth surface and performed quick turns without changing the position [18]. An aerodynamic force-based tail [19] has advantages for continuous turns at very high speed. This bio-inspired solution performs high-performance turning with a simple design solution. However, the method performs well on only smooth surfaces and has limitations in low-speed turning, which is very important for controlling the robot precisely.

This paper suggests a new high-rate turning method for a legged millirobot to perform controllable turning on rough and smooth surfaces. The method is based on cooperation between two modules connected by a compliant joint. The method has very intuitive dynamic motion in which the rear module generates force to help the first module to turn effectively. This method is biologically inspired by some living creatures that help each other to increase mobility [4]. The locomotion is performed in highly dynamic conditions at high speed, so the analysis shows large error due to unexpected conditions. The aim of this research is empirical verification of the cooperative steering method as preliminary research.

Related studies have examined wheeled robots connected by passive joints. Borenstein [20] analyzed the steering of two wheeled modules connected by a linear compliant joint. Adding the joint between the modules allows the robot to achieve small tracking error by preventing slippage of the wheels. Suzuki *et al.* [21] presented wheeled modules with multiple compliant revolute joints between them and performed successful pivot turning. Tilbury *et al.* [22] solved the motion planning of car-like system with trailers by using sinusoidal inputs. Most steering methods for wheeled robots with a compliant joint try to control the wheels precisely to minimize the slip between the wheels and the ground. Our novel cooperative method uses the reaction forces between modules to help the robot turn.

One important and closely related research topic is bio-inspired legged robots with yaw joints, which is a kind of

*This research was supported by the LG Yonam Foundation in 2015.

TaeWon Seo is with the Mechanical Engineering Department, Yeungnam University, Gyeongsan, Republic of Korea. He was with the Department of Electrical Engineering and Computer Sciences, University of California, Berkeley, CA 94720 USA during this research (phone: +82-53-810-2442; fax: +82-53-810-4627; e-mail: taewon_seo@yu.ac.kr).

Carlos S. Casarez and Ronald S. Fearing are with the Department of Mechanical and Electrical Engineering and Computer Sciences, University of California, Berkeley, CA 94720 USA (casarezc@berkeley.edu, ronf@eecs.berkeley.edu).

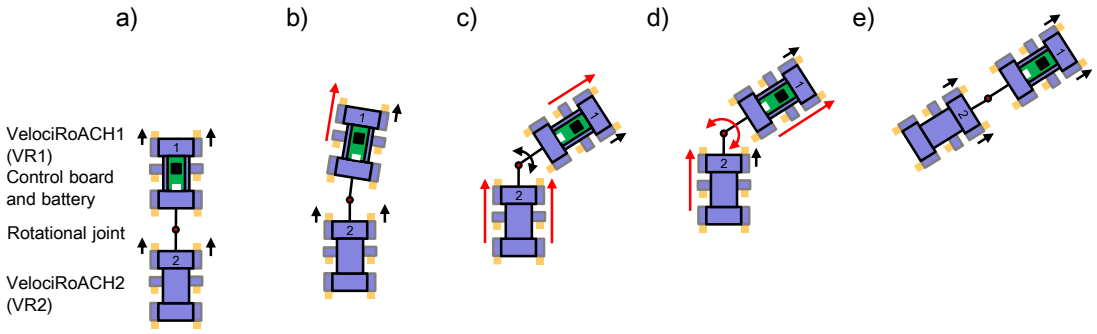


Figure 1. Cooperative turning scenario for two VelociRaACHs (VRs) with a compliant joint. a) The VRs are connected in series using a joint with a torsion spring. b) The front VR does initial turning by increasing the traction force on the left side. c) The rear VR pushes the front VR for fast turning at high speed. d) The linear configuration is recovered by the torsion spring and increasing the traction force on the left side of the rear VR. The traction of the right side of the front VR is increased to maintain the orientation. e) The robot resumes straight line motion in the new direction.

bio-inspired design. Tang *et al.* [22] suggested a hexapod robot with a spine composed of two passive joints between two-legged modules. The design mostly focused on forward movement through spine motion. Inagaki *et al.* [24] proposed a "follow-the-contact–point" gait control method for a centipede-like robot, which can turn by changing the distance between contact points. Recently, Kim [25] examined turning for a biped robot using yaw joint motion. He used dynamic force to steer the biped robot, but the turning was done at very low speed. Our cooperative turning research was done in highly dynamic conditions, so the results can serve as a performance benchmark beyond quasi-statics for legged robot with multiple joints.

This paper is organized as follows. Section 2 explains the cooperative turning method and related expectations. Section 3 presents the design issues of the robot and joint as well as the hardware for control and communication. Section 4 presents experimental results for different operating parameters on different surfaces. The results were quantitatively compared with other turning methods. Concluding remarks and future work then follow.

## II. COOPERATIVE STEERING

### A. Steering scenario

The cooperative turning method is shown in Fig. 1. The method is very intuitive for making the robot turn effectively. Starting from nominal forward running (Fig. 1a), the front robot establishes the turning conditions by speeding up the legs on one side (Fig. 1b). Then, the rear module increases the speed of both the left and right legs to produce a rotational moment on the first module (Fig. 1c). The force from the rear module is transferred through the joint between the modules, which allows the system to generate a sufficiently high moment to steer the robot.

The function of the compliant joint is to make the robot recover a straight configuration. After turning, the velocity of the left and right side are the same for both modules, and the robot changes to a straight configuration from the restoring torque of the compliant joint (Fig. 1d-e). The cooperative approach has several advantages. First, the thrusting force of the rear module can make the whole system turn quickly. Also, due to the multiple contact points of the robot, the robot can turn on surfaces of various materials. The method also facilitates point turns and side walking through the cooperative configuration, which was shown experimentally.

A simple model is required to predict the motion of the robot and analyze the function of the components, although the highly dynamic motion of the robot cannot be predicted precisely using analytical methods. Fig. 2 shows a schematic of the robot during turning. Fig. 2(a) and (b) illustrate turning, and Fig. 2(c) and (d) show the recovery of the straight configuration. The simple force equilibrium equations from the figure are as follows (the signs are defined to make the direction of arrows in Fig. 2 positive):

- Turn module 1 (Fig. 2(a)):

$$\boldsymbol{m}_1 = \boldsymbol{r}_1 \times \boldsymbol{f}_{21} - \boldsymbol{t}_{21} \tag{1}$$

- Turn module 2 (Fig. 2(b)):

$$\boldsymbol{m}_2 = \boldsymbol{r}_2 \times \boldsymbol{f}_{12} + \boldsymbol{t}_{12} \approx \boldsymbol{t}_{12} \tag{2}$$

- Recover module 1 (Fig. 2(c)):

$$\boldsymbol{m}_1 = \boldsymbol{r}_1 \times \boldsymbol{f}_{21} + \boldsymbol{t}_{21} \approx \boldsymbol{t}_{21} \tag{3}$$

- Recover module 1 (Fig. 2(a)):

$$\boldsymbol{m}_2 = \boldsymbol{r}_2 \times \boldsymbol{f}_{12} + \boldsymbol{t}_{21} \tag{4}$$

where $\boldsymbol{m}_i$ is the moment on the $i$-th module, $\boldsymbol{f}_{ij}$ is the reaction force at the joint between the $i$-th module and the $j$-th module, $\boldsymbol{t}_{ij}$ is the compliant restoring force at the joint, and $\boldsymbol{r}_i$ is the perpendicular distance from the center of mass of the $i$-th module to $\boldsymbol{f}_{ij}$. The $\boldsymbol{f}_{ij}$ and $\boldsymbol{t}_{ij}$ are assumed to be perturbations from nominal forces due to traction. Since $\boldsymbol{r}_2$ in (2) and $\boldsymbol{r}_1$ in (3) are very small due to the geometric configuration, they can be assumed to be zero. The gray area in Fig. 2 denotes the region of $\boldsymbol{f}_{21}$ to generate a moment in the positive arrow direction for each module.

Equations (1)–(4) and Fig. 2 have several implications for turning. First, using the initial configuration in Fig. 2, the thrusting force from the rear module will be very helpful for making the robot turn. As shown in (1) and (2), the thrusting force generates a positive moment on the front and rear modules simultaneously. Second, the compliant joint is helpful for turning the rear module, while the joint has an effect in the negative direction on the front module. If the compliant joint is too stiff, it is not easy to steer the robot. Third, the negative thrusting force from the rear module is

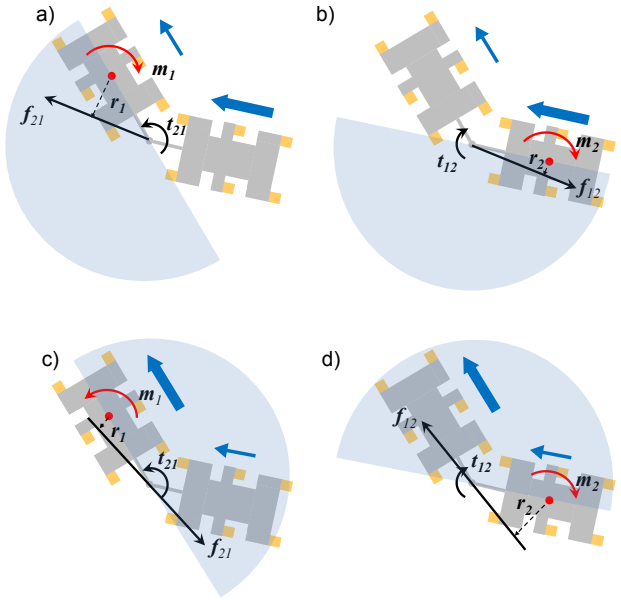


Figure 2. Schematic for the simple analysis of cooperative turning. a, b) Configuration for steering. c, d) Configuration for recovering straight posture. The gray area denotes the region of $f_{21}$ or $f_{12}$ to generate a moment in the indicated direction on the front VR.

helpful for recovering the straight configuration, as shown in (3) and (4). Fourth, the compliant joint is helpful for recovering the straight configuration.

To turn the robot, the front module performs skid steering at low speed to move toward a desired direction, while the rear module pushes the front module with high speed locomotion to turn quickly. To assume a straight configuration after a turn, the rear module slows down relative to the front module to generate a moment with help from the compliant joint. On a low-friction surface, the robot can recover a straight configuration using only the compliant force. The experimental results in the next section demonstrate the effectiveness of the method.

## III. Prototype Design

Fig. 3 shows the assembled prototype of two VelociRoACHs with a compliant joint. The VelociRoACH platform and joint were fabricated by the SCM process, and the legs were fabricated by a molding process. The robot is 300-mm long, 70-mm wide, and weighs 73 g, including the battery. The controller and battery are embedded in the front VelociRoACH platform, and the power and signals are wired by tethers to the rear module.

### A. VelociRoACH

The VelociRoACH platform used in the experiment is the same design used in a previous study [26] except for the flexure material. We used cardboard for the rigid frame and rip-stop nylon for the flexure material. The platform was assembled manually using super glue. Each three feet on the left and right are operated synchronously based on the linkage mechanism shown in Fig. 4, and the robot can achieve a tripod gait or hopping-like gait by changing the phase difference

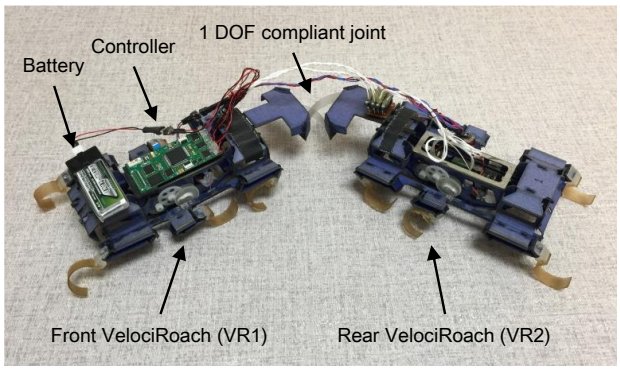


Figure 3. Configuration of two VelociRoaACHs connected by a compliant joint.

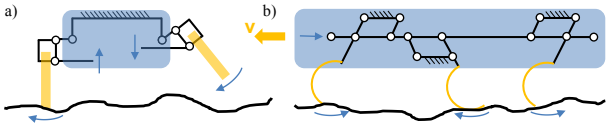


Figure 4. Kinematic configuration of the motion transmission of VR: a) front view and b) side view.

between the left and right feet. Two 7-mm, 3.3-Ω coreless brushed DC motors (Didel # Mk07-3.3) were used to operate the legs, and magnetic rotary encoders were used to control leg position.

### B. Compliant joint

The compliant joint transfers the generated force between the VelociRoACH modules, and the compliance of the joints makes the configuration straight again when the steering is over. There are many candidates for 1-DOF compliant revolute joints, such as a pin joint with a torsional spring, but it is not easy to make it light and easy to assemble.

We designed the compliant joint based on the idea of a cross-spring pivot flexure joint in a precision machine [27]. The joint is composed of two perpendicular leaf springs. The final joint has 1 DOF, and other motions are constrained. Fig. 5(a) shows the template drawing of the joint used for the SCM process, and Fig. 5(b) shows the assembled compliant joint. The compliant joint was implemented on the top of two VelociRoACH modules with sufficient distance between them to prevent the legs from colliding during steering.

Based on the design parameters of the flexure joint, the stiffness of the joint in small deflection can be written as [28]:

$$k_\theta = \frac{8EI\cos\varphi}{H} \tag{5}$$

where $E$ is Young's modulus, $I$ is the area moment of inertia, $2\varphi$ is the angle between flexures, and $H$ is the distance between the fixture and center position of the joint. $k_\theta$ was designed to be $2.69\times10^{-3}$ N·m/rad based on an experiment using $E$ =1 GPa (for PET), $I$ = 0.005 mm$^4$, $\varphi = \pi/4$ rad, and $H$ = 10.5 mm. The compliance parameter is very important for achieving reliable steering performance. However, the parameter used in this study is just for the test and not yet optimized. The stiffness parameter can be adjusted easily by changing the thickness of the PET film.

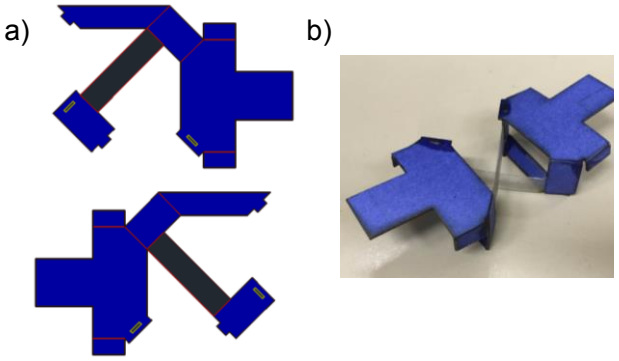


Figure 5. Single-DOF compliant joint made by SCM process. a) 2D design for SCM process, b) assembled compliant joint.

### C. Hardware

The hardware used is very similar to that used in previous research [26]. A single ImageProc 2.5 board [29] was used for the frequency-based feedback control of the four motors (front and rear motors on the left and right). The four motors can be controlled independently through pulse-width modulation of the input voltage. An inertial measurement unit (IMU) is embedded in the ImageProc 2.5 board, and the angular velocity data were used to analyze the results. Zigbee radio communication was used for the data transfer. A 3.7-V, 300-mAh Li-po battery (Nano-tech Inc.) was used as a power source.

## IV. Experimental Results

### A. Experiments on varying speed parameters

To verify the performance of the proposed method, we experimented with various speed conditions on a carpet surface, which is one of the hardest surfaces to turn on stably for legged millirobots. The test was started in extreme conditions, and the results were extended to other surfaces. The frequencies of the four leg sets varied across experiments and the phase of leg sets with equal frequency was fixed according to an alternating tripod gait for each module. The operating frequency was limited to 20 Hz based on previous research [26].

Fig. 6 shows the turning results for various speed conditions. There are several results to be noted from the data. Fig. 6(a) shows pure skid steering, but the desired result is not achieved at all, showing that this method is not good for rough surfaces. By increasing the speed of the rear module, the robot can perform steering as shown in Fig. 6(b). Fig. 6(c) and (d) show results simulating skid steering for the front module while pushing forward with the rear module. The robot achieves very high-speed turning. One difference between Fig. 6(c) and (d) is that the rear module either performs skid steering or pushes forward with high force. The results show that pushing forward by the rear module produces faster turn rates.

The turning direction can be controlled easily by changing the direction of the skid steering of the front module in the setup of Fig. 6(d). One interesting phenomenon is shown in Fig. 6(e) and (f). If the speed of the front and rear modules is similar, the turning rate is measured similarly. However, at different running speeds of the robot, the turning radius of

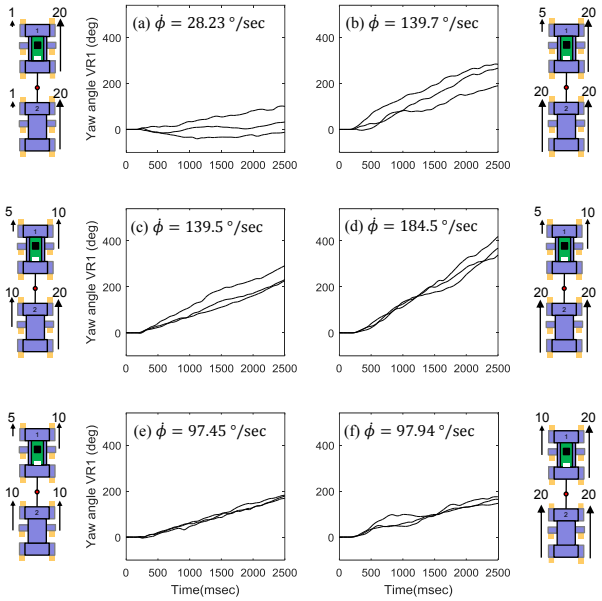


Figure 6. Experimental results for various moving speed. The numbers on the robot diagram denote the operating frequency of the legs of the modules. Three trials were conducted per condition. Numbers above plots indicate average yaw rates during the steering period.

curvature will be different. Details about the steering posture are summarized in the Multimedia Extension.

### B. Experiments on different material surfaces

Carpet, paper, and smooth tile surfaces were selected for additional experiments. The carpet has the highest frictional estimated coefficient, while the floor has the lowest. Based on the results on carpet, we used three different velocities for the left and right legs.

Fig. 7 shows the results of the experiment (please see the Multimedia Extension for details). The robot can turn reliably on the three different surfaces, and the skid-steering method for the front with pushing forward by the rear module produces the best turning performance on all three surfaces. The angular velocity was very consistent on the paper surface. In our experience, paper is the most reliable surface for the VelociRoACH platform to turn well [12] because of the sufficient isotropic friction characteristics.

The low-speed result on the tile floor is shown in the top right of Fig. 7. The turning rate is lowest due to the low friction of the surface, and the rate increases dramatically when the speed of the robot is increased. From the results, we conclude that there is a different threshold for the robot to achieve a desired turn rate on surfaces with different friction. The optimal operating conditions and online measurement of the frictional conditions remain as future work.

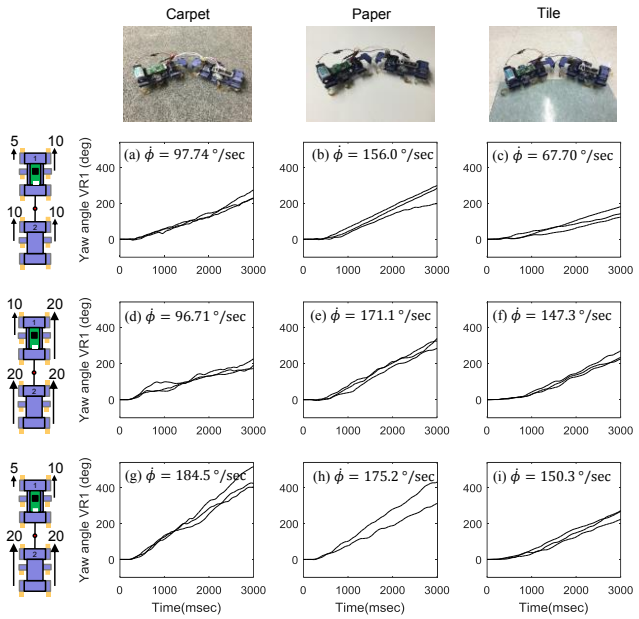


Figure 7. Experiment results on carpet, paper, and smooth tile surfaces. Different velocities were used for each row with different surfaces for each column. The numbers on the robot diagram denote the operating frequency of the legs. Three trials per conditions. Numbers above plots indicate average yaw rates during the steering period.

One popular measure for comparing the turning performance of legged robots is "maneuverability" $\dot{\phi}v$ (angular velocity × speed), which denotes how well the robot can turn at high speed. The comparison results of the proposed method are summarized in Table I. The index is calculated from the average angular velocity measured by the ImageProc 2.5 board and measured radius of turning ($=\dot{\phi}^2 r$). Differential drive for a single VelociRoACH on a paper surface was performed for a reference data, which is shown in Table I. The proposed method shows high turning performance and works well on different surfaces. In contrast, the results of the other robots were mostly measured on a specific surface with good conditions for the turning method. The degree of control in Table I denotes how many motors are used to control each motor, and our method has a lower degree of control compared to the other robots.

TABLE I. COMPARISON OF LEGGED TURNING PERFORMANCE (REORGANIZED FROM [12] AND [30])

| Robot | Surface | #Leg (A) | #Act -uator (B) | Degree of control (B/A) | $\dot{\phi}v$ (°ms$^{-2}$) |
|---|---|---|---|---|---|
| iSprawl | stone | 6 | 3 | 0.50 | 50.0 |
| HAMR | paper | 4 | 6 | 1.50 | 37.5 |
| OctoRoACH | carpet | 8 | 2 | 0.25 | 36.0 |
| SailRoACH | carpet | 6 | 3 | 0.50 | 134 |
| VelociRoACH roll-turn 5Hz | tile | 6 | 2 | 0.33 | 29.1 |
| VelociRoACH diff.-drive 5/10Hz | paper | 6 | 2 | 0.33 | 40–60 |
| *This work* | *carpet paper tile* | *12* | *4* | *0.33* | *40–60 100–120 60–80* |

## C. *Possibility of dexterous motion*

Other locomotive methods can be considered in addition to turning for dexterous two-module driving with a compliant joint. Fig. 8 shows one of possibility of side-walking locomotion, which can be done by driving the front and rear modules in opposite directions with different speed. The VelociRoACH platform is a nonholonomic system, but the side-walking can make the system holonomic, which is very helpful for planning the motion trajectory of the robot.

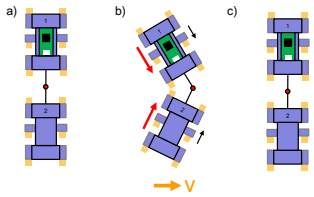


Figure 8. Scenario of side walking. a) Two VelociRoACHs (VRs) are connected in series using a joint with a torsion spring. b) The VR performs side-walking by inward differential driving. c) The robot changes position in the lateral direction without steering.

Fig. 9 shows the results of the side-walking method. The side-walking method worked well on a wooden surface and generated enough sideways thrusting force (Fig. 9(a–d)). However, on carpet, the side-walking locomotion generates torque that makes the robot turn (Fig. 9(e–h)). This is because of the friction anisotropy due to the shape of the legs, and the effect is not severe on the wooden surface. Therefore, the estimation of friction is very important for dexterous motion but less important in steering. Many interesting tactile sensors have been developed recently to estimate friction [1, 31], and we are going to adopt the sensors in the future.

As shown in Fig. 9(e–h), the robot can also perform point turns by thrusting the front legs backward to generate force to maintain the position of the front module. This kind of locomotion method is also very helpful for following arbitrary paths.

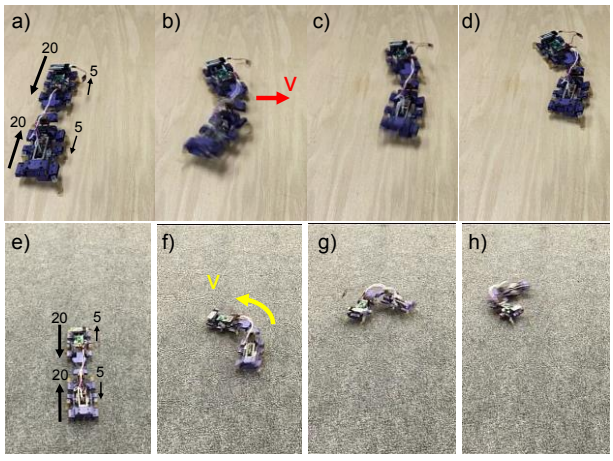


Figure 9. Experimental results for the side-walking method on different surfaces: (a)-(d) wood, (e)-(h) carpet. The numbers and arrow direction on the robot denote the operationing frequency and moving direction of the legs.

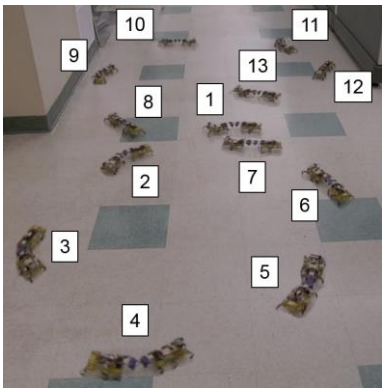


Figure 10. Selected video frames from the closed-loop steering experiment on tile shown in Fig. 11 (frames are spaced 1 second apart).

### *D. Closed-loop steering experiments*

The following experiments were performed using a slightly modified robot. This robot is functionally equivalent but uses VelociRoACH robots made with a polycarbonate structure and rip-stop nylon flexures. The control board is mounted on the back robot instead of on the front and encoders are used to control the leg trajectories of only the back robot. The transmissions of the robots, the joint connecting the robots, and the battery mounting location are the same as in previous experiments. The total mass of the modified robot is 75 g.

For closed-loop steering experiments, angular velocity data was collected with the gyroscope on the rear robot VR2 as feedback for a steering controller. The raw gyro rate data exhibits high-frequency vibrations from the leg motions of the robot and is filtered by averaging over a 50 msec window to produce the measurement $\dot{\phi}_{meas}$. The yaw measurement $\phi_{meas}$ is computed by integrating the raw gyro signal in time.

The steering controller is constructed following the differential drive strategy in [11]. In the open-loop experiments, skid steering with the front robot while pushing straight with the rear robot produced the most effective turning, so this strategy is employed in closed-loop form using the ImageProc 2.5 onboard the robot. Given a target yaw velocity $\dot{\phi}_r$, the controller adjusts the duty cycle of each leg side of the front robot VR1 to steer the connected robot. The target yaw trajectory $\phi_r$ is computed by integrating $\dot{\phi}_r$ in time. The controller has two contributing terms—a proportional term based on yaw rate error and an integral term based on yaw angle error. The output of the controller is as follows:

$$u = -K_P\left(\dot{\phi}_{meas} - \dot{\phi}_r\right) - K_I(\phi_{meas} - \phi_r) \qquad (6)$$

where the control signal $u$ is the increase in the right motor duty cycle $u_R$ of VR1 relative to the left motor duty cycle $u_L$, and duty cycle has units of PWM. If $u$ is negative, $u_L$ increases relative to $u_R$. The duty cycle of each motor of VR1 is fixed to be strictly positive, and ranges over 0-4096 PWM. For the following experiments, $K_P = 19.2$ PWM/(deg/s) and $K_I = 6.25$ PWM/deg.

The steering controller fixes the duty cycle of a given leg side at a nominal value $u_{nom}$ during steering towards that side. For the following experiments, $u_{nom} = 1200$ PWM. There is also a feedforward term $K_{ff}$ in the controller that biases the motor duty cycles to make the robot steer near the desired turn rate under no control input. For example with positive $\dot{\phi}_r$, when $u = 0$, $u_R = u_{nom} + K_{ff}$ and $u_L = u_{nom}$. For the following experiments, $K_{ff} = 1800$ PWM.

Selected video frames of a closed-loop steering experiment are shown in Fig. 10, with control data plotted in Fig. 11. In this experiment, the connected robot follows a "figure 8" trajectory on tile, with a commanded turning speed of 60 deg/sec during each segment. In these experiments, the rear robot is commanded to have a stride frequency of 15 Hz for both leg sets. The duty cycle of the front robot's leg sets (scaled from 0-4096 PWM to 0-100%) is controlled based on yaw rate and angle measurements to steer about the target trajectory. The robots track the trajectory with an average yaw error of 2.2° with a maximum error of 56° at a time of 8480 msec. The large oscillations around the target trajectory may be explained by varying friction over the tile surface, which imparts disturbances to the steering. Also, the spring and damping properties of the connection between the robots may amplify oscillations during dynamic turning under the tested high-speed turning conditions with switching turn direction.

As a comparison to open-loop turning performance, the turn radius of the robot during this closed-loop experiment was estimated from the video frames to be 0.6 m (the tiles are 1 foot by 1 foot). With a nominal turning rate of 60 deg/sec, this corresponds to a maneuverability of 75 $°ms^{-2}$, which is within the range of connected robot values on tile in Table I.

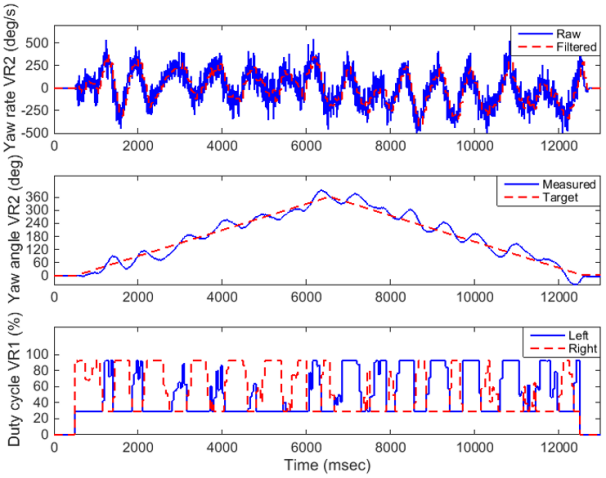


Figure 11. Representative closed-loop steering results with the robot tracking a "figure 8" turning trajectory on tile. The commanded turning speed during each segment is 60°/sec. The commanded stride frequency of each leg set of the rear robot VR2 was set to 15 Hz.

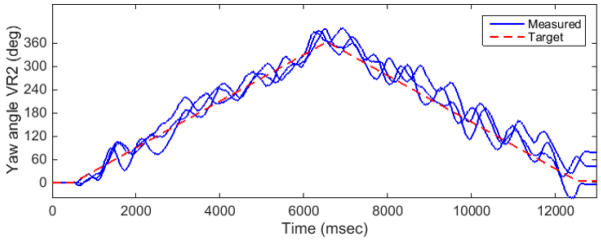


Figure 12. Yaw trajectories from three closed-loop steering experiments with the robot tracking a "figure 8" turning trajectory on tile.

To demonstrate repeatability of the closed-loop turning results on tile, the experiment was run for three total trials. The yaw trajectories for these repeated tests are shown in Fig. 12. The yaw trajectories have similar tracking performance as the representative trial in Fig. 11.

## V. Conclusion

This study has proposed a new high-rate turning method for a legged millirobot, which can produce turns across different surfaces. The VelociRoACH platform was used with a controller, and two VelociRoACH modules were connected by a compliant joint manufactured by the SCM process. The robot can turn fast on surfaces with various roughness using the reaction force generated between the two modules.

For future work, path planning is required for the nonholonomic robotic platform to complete a given mission, and tracking control should be done to make the robot trace a predefined path. The side-walking experiments and closed-loop steering experiments tracking a "figure 8" trajectory on tile are first steps towards this goal. Optimal design of components such as the stiffness of the compliant joint are required to improve steering performance. In addition, proper selection of control parameters such as leg frequencies based on estimation of the friction coefficient [31] could improve adaptability of the method to different terrain types. The turning method could be extended to autonomous planning for a legged robot in search and rescue missions.

## Acknowledgment

The authors thank the members of the Biomimetic Millisystems Laboratory at UC Berkeley for valuable discussions and comments, and Mr. HyunGyu Kim for video editing.

## References

[1] D. W. Haldane, C. S. Casarez, J. T. Karras, J. Lee, C. Li, A. O. Pullin, E. W. Schaler, D. Yun, H. Ota, A. Javey, R. S. Fearing, "Integrated manufacture of exoskeletons and sensing structures for folded millirobots," *ASME J. of Mechanisms and Robotics*, vol. 7, no. 2, 2015, 021011.

[2] D. W. Haldane, R. S. Fearing, "Running beyond the bio-inspired regime," in Proc. *IEEE Int'l Conf. on Robotics and Automation*, Seattle, 2015, pp. 4539-4546.

[3] P. Birkmeyer, K. Peterson, R. S. Fearing, "DASH: A dynamic 16g hexapedal robot," in Proc. *IEEE/RSJ Int'l Conf. on Intelligent Robots and Systems*, St. Louis, 2009, pp. 2683-2689.

[4] C. S. Casarez, R. S. Fearing, "Step climbing cooperation primitives for legged robots with a reversible connection," in Proc. *IEEE Int'l Conf. on Robotics and Automation*, Stockholm, 2016, pp. 3791-3798.

[5] D. Haldane, P. Frankhauser, R. Siegwart, R. Fearing, "Detection of slippery terrain with a heterogeneous team of legged robots," in Proc. *IEEE Int'l Conf. on Robotics and Automation*, Hong Kong, 2014, pp. 4576-4581.

[6] C. J. Rose, P. Mahmoudieh, R. S. Fearing, "Coordinated launching of an ornithopter with a hexapedal robot," in Proc. *IEEE Int'l Conf. on Robotics and Automation*, Seattle, 2015, pp. 4029-4035.

[7] T. Yoshida, K. Nagatani, S. Tadokoro, T. Nishimura, E. Koyanagi, "Improvements to the rescue robot quince toward future indoor surveillance missions in the Fukushima Daiichi nuclear power plant," *Field and Service Robotics*, vol. 92, 2013, pp. 19-32.

[8] A. M. Hoover, R. S. Fearing, "Fast scale prototyping for folded millirobots," in Proc. *IEEE Int'l Conf. on Robotics and Automation*, Pasadena, 2008, pp. 886-892.

[9] A. T. Baisch, R. J. Wood, "Pop-up assembly of a quadrupedal ambulatory microrobot," in Proc. *IEEE/RSJ Int'l Conf. on Intelligent Robots and Systems*, Tokyo, 2013, pp. 1518-1524.

[10] K. L. Hoffman, R. J. Wood, "Passive undulatory gaits enhance walking in a myriapod millirobot," in Proc. *IEEE/RSJ Int'l Conf. on Intelligent Robots and Systems*, San Fransisco, 2011, pp. 1479-1486.

[11] A. O. Pullin, N. J. Kohut, D. Zarrouk, and R. S. Fearing, "Dynamic turning of 13 cm robot comparing tail and differential drive," in Proc. *IEEE Int'l Conf. on Robotics and Automation*, Minneapolis, 2012, pp. 5086-5093.

[12] D. W. Haldane, R. Fearing, "Roll oscillation modulated turning in dynamic millirobots," in Proc. *IEEE Int'l Conf. on Robotics and Automation*, Hong Kong, 2014, pp. 4569-4576.

[13] J. S. Lee, R. S. Fearing, "Anisotropic collapsible leg spines for increased millirobot traction," in Proc. *IEEE Int'l Conf. on Robotics and Automation*, Seattle, 2015, pp. 4547-4553.

[14] T. Libby, T. Y. Moore, E. Chang-Siu, D. Li, D. J. Cohen, A. Jusufi, R. J. Full, "Tail-assisted pitch control in lizards, robots and dinosaurs," *Nature*, vol. 481, pp. 181-184, 2012.

[15] A. De, D. E. Koditschek, "Parallel composition of templates for tail-energized planar hopping," in Proc. *IEEE Int'l Conf. on Robotics and Automation*, Seattle, 2015, pp. 4562-4569.

[16] H. Kim, D. G. Lee, T. Seo, "Rolling stability enhancement via a balancing tail for water-running robots," *Journal of Bionic Engineering*, vol. 12, no. 3, pp. 395-405, 2015.

[17] T. Seo, M. Sitti, "Tank-like module-based climbing robot using passive compliant joints," *IEEE-ASME Transaction on Mechatronics*, vol. 18, no. 1, pp. 397–408, 2013.

[18] N. J. Kohut , A. O. Pullin, D. W. Haldane, D. Zarrouk, R. S. Fearing, "Precise dynamic turning of a 10 cm legged robot on a low friction surface using a tail," in Proc *IEEE Int'l Conf. on Robotics and Automation*,, Karlsruhe, 2013, pp. 3299–3306.

[19] N. J. Kohut, K. C. Peterson, R. S. Fearing, "Aerodynamic Steering of a 10 cm High-Speed Running Robot," in Proc. *IEEE/RSJ Int'l Conf. on Intelligent Robots and Systems*, Tokyo, 2013, pp. 5593-5599.

[20] J. Borenstein, "Control and kinematic design of multi-degree-of-freedom mobile robots with compliant linkage," *IEEE Transaction on Robotics and Automation*, vol. 11, no. 1, pp. 21-35.

[21] K. Suzuki, A. Nakano, G. Endo, S. Hirose, "Development of multi-wheeled snake-like rescue robots with active elastic trunk," in Proc. *IEEE/RSJ Int'l Conf. on Intelligent Robots and Systems*, Algarve, 2012, pp. 4602-4607.

[22] Y. Tang, S. Ma, Y. Sun, D. Ge, "Planar legged walking of a passive-spine hexapod robot," *Advanced Robotics*, vol. 29, no. 23, pp. 1510-1525, 2015.

[23] S. Inagaki, T. Niwa, T. Suzuki, "Follow-the-contact-gait control of centipede-like multi-legged robot to navigate and walk on uneven terrain," in Proc. *IEEE/RSJ Int'l Conf. on Intelligent Robots and Systems*, Taipei, 2010, pp. 5341-5346.

[24] D. Tilbury, J. P. Laumond, R. Murray, S. Sastry, G. Walsh, "Steering car-like systems with trailers using sinusoids," In Proc *IEEE Int'l Conf. on Robotics and Automation*, Nice, 1992, pp. 1993-1998.

[25] J. Kim, *Design and Analysis of a Lizard-Inspired Legged Robot*, Ph.D. Thesis, Seoul National Univesrity, 2015.

[26] D. W. Haldane, K. C. Peterson, F. L. Garcia Bermudez, R. S. Fearing, "Animal-inspired design and aerodynamic stabilization of a hexapedal millirobot," in Proc *IEEE Int'l Conf. on Robotics and Automation*,, Karlsruhe, 2013, pp. 3279–3286.

[27] T. J. Teo, G. Yang, I.-M. Chen, *Compliant Manipulators*, Handbook of Manufacturing Engineering and Technology, Spring-Verlog, 2014.

[28] X. Pei, J. Yu, G. Zong, S. Bi, "An effective pseudo-rigidi-body method for beam-based compliant mechanisms," *Precision Engineering*, vol. 34, pp. 634-639, 2010.

[29] S. S. Baek, F. L. Garcia Bermudez, R. S. Fearing, "Flight control for target seeking by 13 gram ornithopter," in Proc. *IEEE/RSJ Int'l Conf. on Intelligent Robots and Systems*, 2011, pp. 2674–2681.

[30] D. Zarrouk, D. W. Haldane, R. S. Fearing, "Dynamic legged locomotion for palm-size robots," in Proc. *SPIE Micro- and Nanotechnology Sensors, Systems, and Applications VII*, 2015.

[31] *Tactile sensing for small legged robots-bipedal running experiment*, https://www.youtube.com/watch?v=NbAZ9zsMRLQ (retrieved at Feb. 8, 2016).